Title no. 96-M83

# Harmonized Test Procedures for Steel Fiber-Reinforced Concrete

by Peter Marti, Thomas Pfyl, Viktor Sigrist, and Tomaz Ulaga

A circular slab test method is described as an alternative to modulus of rupture and square slab tests for steel fiber-reinforced concrete. Results of 20 modulus of rupture, 12 square slab, and 24 circular slab tests are compared based on a general theoretical approach that accounts for the random fiber distribution and the successive softening by fiber pullout. Existing requirements for modulus of rupture and square slab tests are reviewed, and harmonized procedures for these as well as the circular slab tests are proposed. It is suggested to use an effective flexural tensile strength and a fracture energy parameter to characterize the strength and toughness of steel fiber-reinforced concrete. Furthermore, an acceptance criterion is introduced, aiming at excluding materials with a too drastic softening.

Keywords: bond (concrete to reinforcement); cracking (fracturing); ductility; fiber reinforcement; shotcrete; strength; tests.

# INTRODUCTION

Steel fiber-reinforced concrete has increasingly been used in recent years, primarily for tunnel linings, industrial floor slabs, and similar applications. Normally, fiber lengths and diameters are of the order of 30 and 0.5 mm, respectively, and fiber contents range from approximately 20 to 100 kg/ m<sup>3</sup> of concrete, with typical values approximately 40 kg/m<sup>2</sup> of concrete. Unlike ordinary reinforced concrete with an appropriate minimum reinforcement, such fiber contents do not ensure a narrow crack spacing, and a softening response is observed after cracking. Compared to plain concrete, however, the ductility is significantly increased because the fibers continue to transmit forces across the cracks. Typically, failure is characterized by fiber pullout; fiber failures may occur for relatively long fibers and high concrete strengths.

In the past, modulus of rupture tests<sup>1-3</sup> as well as square slab tests<sup>4</sup> have been used to determine strength and ductility properties of steel fiber-reinforced concrete. Unfortunately, the modulus of rupture tests exhibit considerable scatter and the square slab tests are not straightforward to analyze. In addition, there are significant differences among the test procedures required by different standards<sup>1-3</sup> and, apparently, no attempt has yet been made to relate the two test methods based on a general theoretical approach.

The present paper describes an alternative circular slab test method for steel fiber-reinforced concrete. 5,6 Results of 24 circular slab tests are compared with those of 20 corresponding modulus of rupture tests and 12 square slab tests. The comparison is based on a theoretical approach that accounts for the random fiber distribution and the successive softening by fiber pullout. In conclusion, harmonized test procedures are proposed for the three test methods.

Table 1—Dimensions of test specimens<sup>\*</sup>

Test	a	b	c	h	1
R, modulus of rupture	_	100	75	100	450
S, square slab	100	520	40	100	_
C, circular slab	120	680	60	100	_

**Table 2—Mixture properties** 

Mixture	1	2	3	4	Units
Aggregate type	Natural and crushed			Crushed	_
$d_{max}$	16		8		mm
Cement type	Normal hardening		Rapid hardening		_
Cement content	420		425		kg/m <sup>3</sup>
$f_c'$	35		45		MPa
Fiber content	40	90	40	50*	kg/m <sup>3</sup>
Application	Cast-in-place			Shotcrete	_

<sup>\*</sup>Fiber content in concrete mixer.

### RESEARCH SIGNIFICANCE

The circular slab tests result in little scatter and are easy to execute and analyze, providing a valuable alternative to the modulus of rupture and square slab tests. The theoretical approach presented in this paper allows for a harmonization of the three test methods.

### **EXPERIMENTS**

Figure 1 illustrates the test principles of the three types of experiments performed in the present investigation.<sup>5,6</sup> Corresponding dimensions are summarized in Table 1.

Four different concrete mixtures were used (see Table 2). For each mixture, five modulus of rupture tests (R) and six circular slab tests (C) were performed. In addition, Mixture 1 was used for 12 square slab test specimens (S). The same type of steel fiber with hooked ends was used for all experiments (see Fig. 2).

Whereas the modulus of rupture tests were performed in a universal testing machine, the slab tests were conducted in specially assembled steel frames. Loads were applied by hydraulic jacks in a deformation controlled manner. Applied loads F and corresponding displacements w were continuously monitored by load cells and linearly variable displacement transducers, respectively. Bearing friction effects were

ACI Materials Journal, V. 96, No. 6, November-December 1999.

ACI Materiats Journal, v. 96, No. 6, November-December 1999. Received October 14, 1998, and reviewed under Institute publication policies. Copyright © 1999, American Concrete Institute. All rights reserved, including the making of copies unless permission is obtained from the copyright proprietors. Pertinent discussion including author's closure, if any, will be published in the September-October 2000 ACI Materials Journal if the discussion is received by June 1, 2000.

ACI member Peter Marti is a professor of structural engineering at ETH, Zurich, Switzerland. His research interests include modeling of structural behavior and design.

**Thomas Pfyl** is a research associate at the Institute of Structural Engineering of ETH. His research interests include minimum reinforcement of structural concrete and steel fiber-reinforced concrete.

**Viktor Sigrist** obtained a DrScTechn degree from ETH in 1995. He is a partner of Ritz Zimmerli Sigrist AG, consulting engineers in Lucerne, Switzerland.

**Tomaz Ulaga** is a research associate at the Institute of Structural Engineering of ETH. His research interests include the evaluation and strengthening of concrete bridges.

reduced as much as possible by using timber strips and small teflon bearings along the support lines for the square and circular slab tests, respectively. The displacements at the loading points were increased at rates of approximately 0.2 and 1.5 mm/min for the modulus of rupture and slab tests, respectively.

Figure 3 shows typical crack patterns for the square and circular slab tests. Four to six cracks formed for the square slab specimens, while five to six cracks occurred for the circular slab specimens. Compared to ordinary reinforced concrete, the small number of cracks is remarkable. It can be explained by the inherent softening response, resulting in a pronounced deformation localization after cracking.

Figures 4 through 6 present the results of the different tests. Note that for the modulus of rupture tests, the average deflection of the two loading points w equals  $w_m l l (3x)$  if only deformations due to hinge rotation are taken into account, where  $w_m$  = deflection at midspan, l = span length, and x = distance

of flexural hinge from nearer support ( $l/3 \le x \le l/2$ ) (see Fig. 1(a)). For the square and circular slab tests the deflections w correspond to the deflections of the steel loading plates relative to the supports. In the lower diagrams in Fig. 4 through 6, the integral

$$W = \int_{0}^{w} F dw \tag{1}$$

is plotted versus w.

### **THEORY**

# **Uniaxial tension**

Randomly oriented straight fibers having a length  $l_f$  and a circular cross section with a diameter  $d_f$  corresponding to a volumetric reinforcement ratio  $\rho_f$  are considered. Noting that the center of gravity of a hemispherical surface of radius 1 is located at a distance of 1/2 above its base, it can be seen that the effective reinforcement ratio in any direction  $l^0$  equals to  $\rho_f/2$ . Introducing a unit crack surface with a monotonically increasing crack opening u (Fig. 7(a)), and assuming a pure fiber pullout on the side of the shorter embedment length of any fiber crossing the crack one achieves for u = 0, an initial stress

$$\sigma_0 = \frac{\rho_f l_f \tau_b}{2d_f} \tag{2}$$

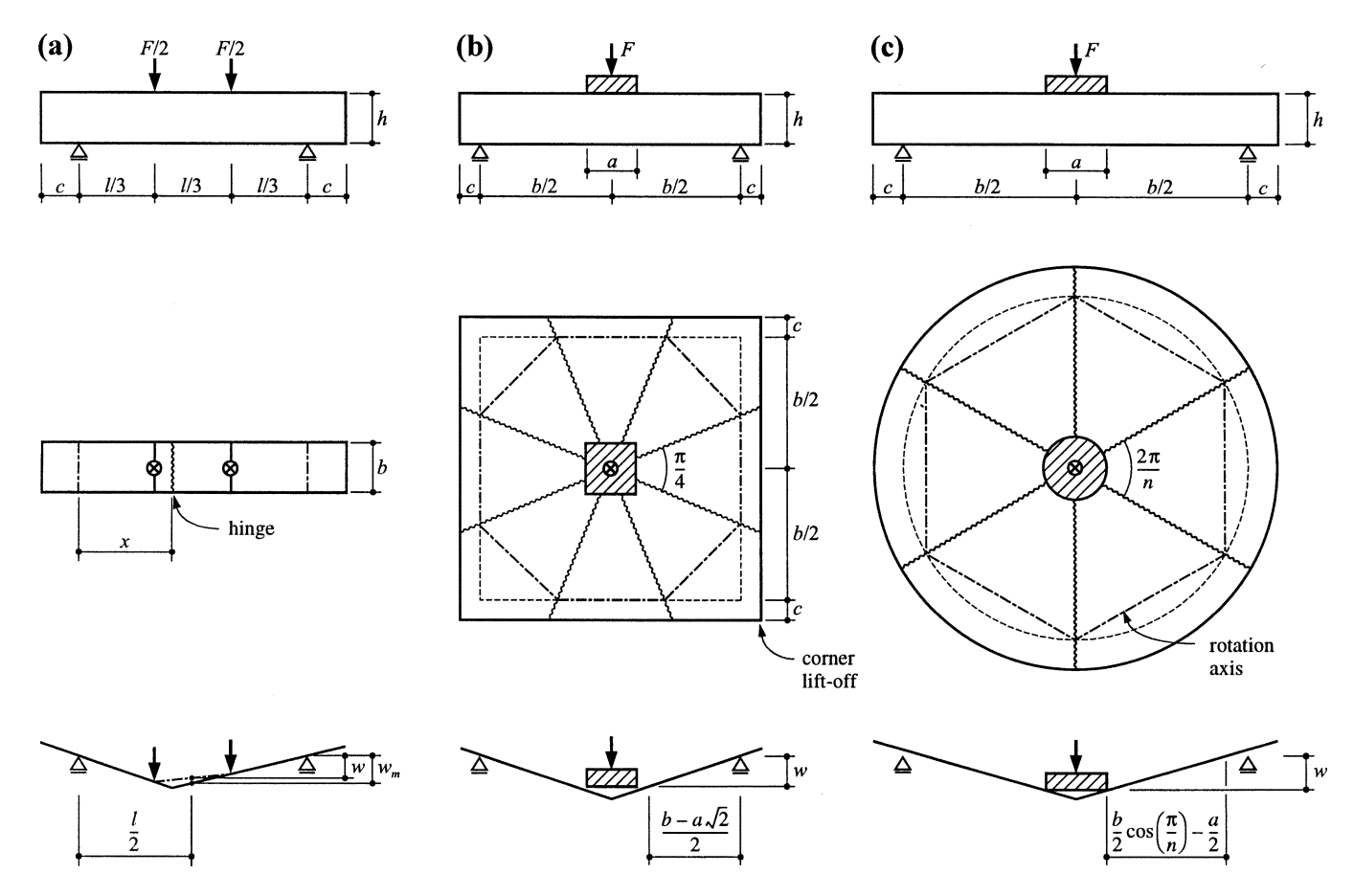


Fig. 1—Test principles and failure mechanisms: (a) modulus of rupture test; (b) square slab test; and (c) circular slab test.

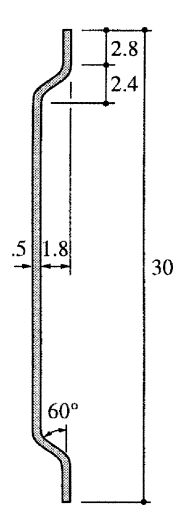


Fig. 2—Fiber used in present investigation. (Note: dimensions in mm.)

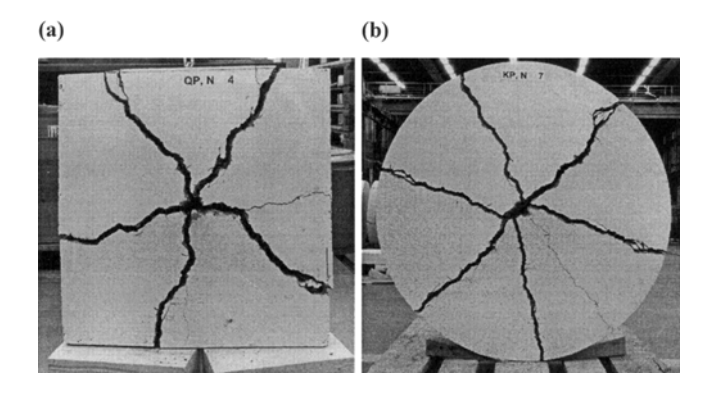


Fig. 3—Typical crack patterns: (a) square slab test, n = 5; and (b) circular slab test, n = 6.

if one assumes a constant bond shear stress  $\tau_b$  and equates the specific work increment  $\sigma_0 du$  to the corresponding specific dissipation  $(\tau_b \pi d_f l_f / 4) du(\rho_f / 2) / (d_f^2 \pi / 4)$ , where  $l_f / 4$  = average pullout length for u = 0. With increasing crack opening, more and more fibers are fully pulled out and, for  $u = l_f / 2$ , the stress drops to zero. Because the number of bonded fibers decreases linearly with increasing u, one obtains, for  $0 \le u \le l_f / 2$ , the parabolic relationship

$$\sigma = \sigma_0 \left( 1 - \frac{2u}{l_f} \right)^2 \tag{3}$$

See Fig. 7(b). The integral under the parabola is equal to the specific fracture energy

$$G_f = \frac{\sigma_0 l_f}{6} = \frac{\rho_f l_f^2 \tau_b}{12 d_f}$$
 (4)

### Remarks

Equations (2) and (3) are due to Hartwich.<sup>7</sup> The parabolic decrease of  $\sigma$  according to the rigid-softening plastic relationship (Eq. (3)) is well confirmed experimentally by Körmeling<sup>8</sup> and Shah et al.<sup>9</sup>

For a plane rather than a spatial random distribution of the fibers, the effective reinforcement ratio  $\rho_f/2$  in Eq. (2) should be replaced by  $2\rho_f/\pi$  because the center of gravity of a half-circle of radius 1 is located at a distance of  $2/\pi$  above its base diameter. <sup>10</sup> Shotcrete application may lead to a nearly plane fiber orientation.

The present considerations focus on the softening response after cracking of the concrete. Depending on the fiber geometry and the bond properties, a crack opening of approximately 0.05 mm is required to develop the maximum fiber stresses. While the initial behavior up to the maximum fiber stresses could also be analyzed assuming a constant bond shear stress, <sup>7</sup> this is of little relevance in the present context.

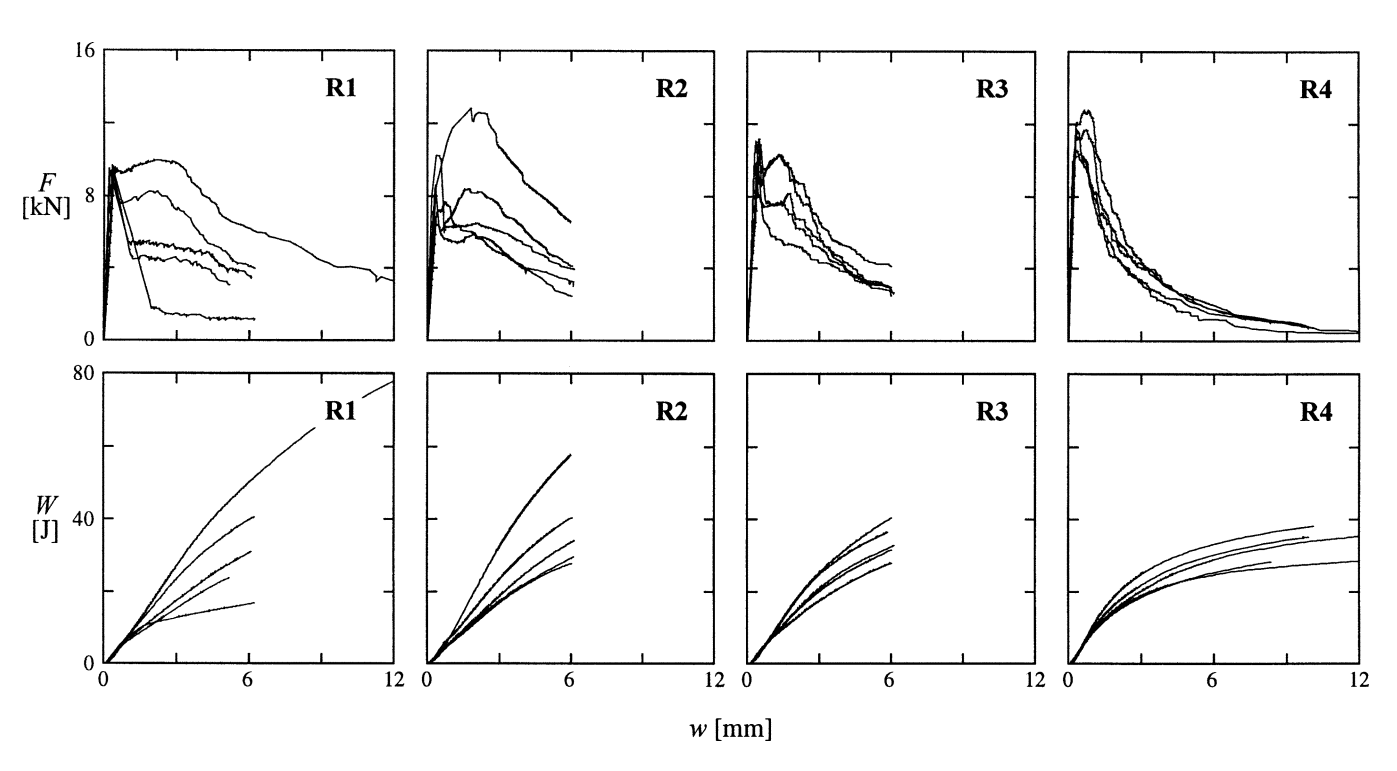


Fig. 4—Results of modulus of rupture tests.

Tests showed <sup>10-12</sup> that the angle between the crack surface and the fiber has only a little influence on the pullout force. A recent investigation <sup>13</sup> demonstrated that, while there is a considerable effect of fiber geometry and angle of pullout for smaller crack openings, these effects tend to diminish for large crack openings. Experimental evidence also shows that the frictional slip between fiber and concrete corresponds to a thin fracture zone around the fiber; the fracture zone has a thickness of only a few micrometers <sup>14</sup> and its properties can only approximately be related to the concrete strength. <sup>15</sup>

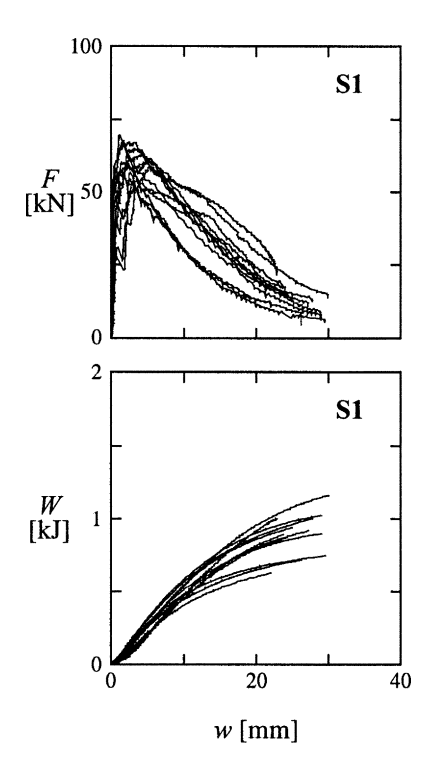


Fig. 5—Results of square slab tests.

Thus, while there seems to exist sufficient experimental justification for the assumption of a constant bond shear stress, <sup>11,12,16</sup> its magnitude is not easy to assess. As an approximation, the value

$$\tau_b = 2f_{ct} = 0.6(f_c')^{2/3} \tag{5}$$

in MPa units will be used herein. This value has successfully been applied to investigate a broad range of problems of cracking, minimum reinforcement, and ductility of structural concrete members. <sup>17-19</sup>

Note that, according to Eq. (2) and (5), the initial stress  $\sigma_0$  becomes equal to the product of the volumetric reinforcement ratio  $\rho_f$ , the shape factor  $l_f/d_f$ , and the concrete tensile strength  $f_{ct}$ , that is,  $\sigma_0 = \rho_f (l_f/d_f) f_{ct}$ .

To compare the specific fracture energy according to Eq. (4) with that of plain concrete, consider a mixture with  $f_c' = 30$  MPa containing 40 kg of steel fibers per m³ of concrete, characterized by  $l_f = 30$  mm and  $d_f = 0.5$  mm. With the steel density of 7850 kgm³, Eq. (4) and (5) yield  $G_f = 40 \times 30^2 \times 0.6 \times 30^{2/3}/(12 \times 0.5 \times 7850) = 4428 \text{ Nm}^{-1}$ . For the plain concrete one may assume a linear softening from  $f_{ct}$  to zero at a crack opening of  $0.025 \times d_{max}^{1/4}$  (in mm), where  $d_{max} = \text{maximum aggregate}$  diameter. Thus, for  $d_{max} = 16$  mm,  $G_f = 0.3 \times 30^{2/3} \times 0.025 \times 16^{1/4} = 72 \text{ Nm}^{-1}$ , that is, only 1.6% of the value for the steel fiber-reinforced concrete.

# Flexure—General analysis

The flexural hinge in a member of depth h shown in Fig. 8(a) is characterized by the compression zone depth z and the hinge rotation  $\theta$ . Assuming a compressive stress of  $0.85f_c'$  over 80% of the depth z, introducing the crack opening parameter  $\xi$  with

$$\theta(h-z) = \frac{\xi l_f}{2} \tag{6}$$

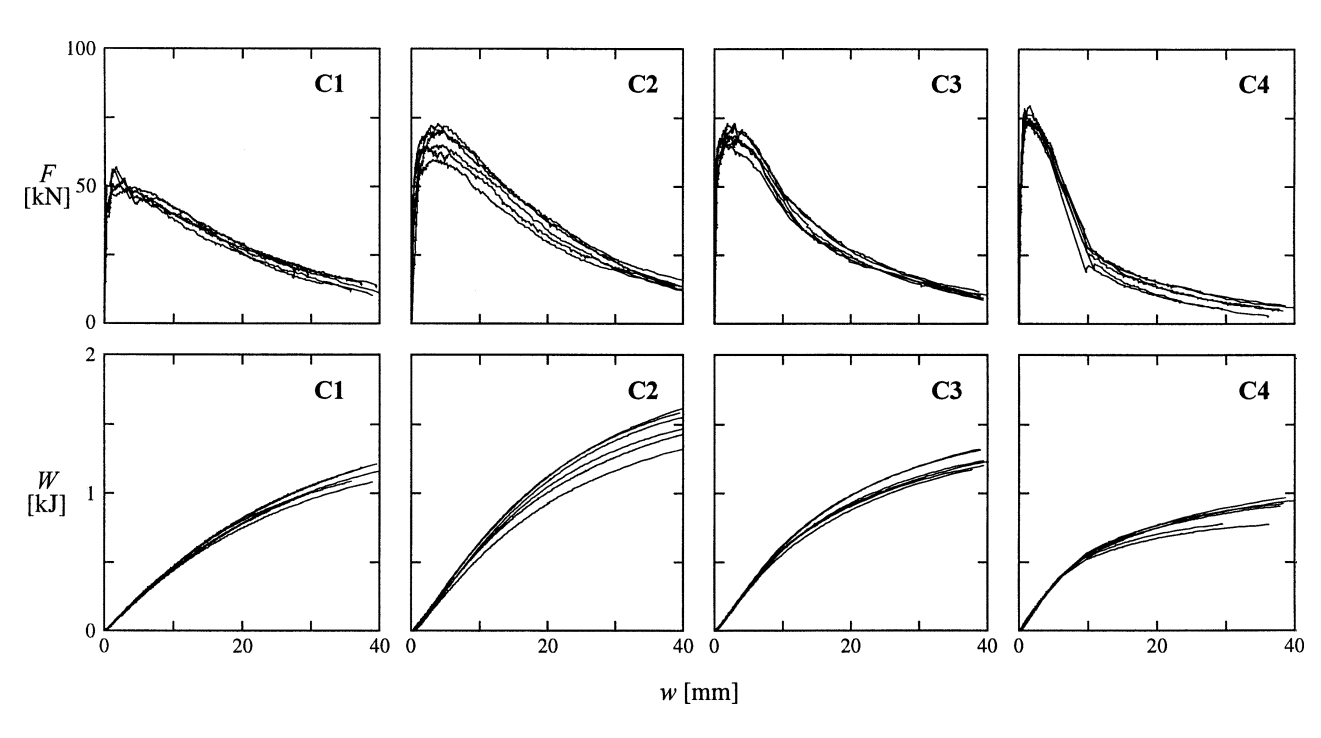


Fig. 6—Results of circular slab tests.

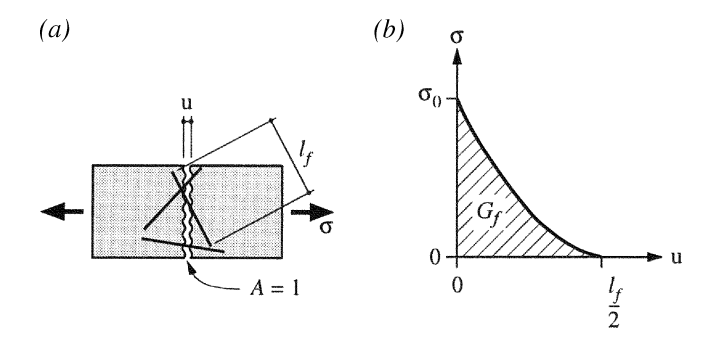
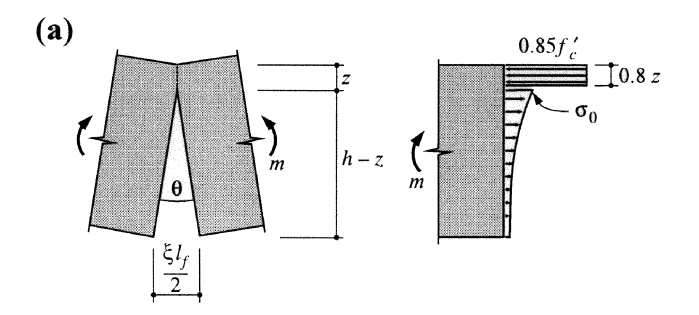
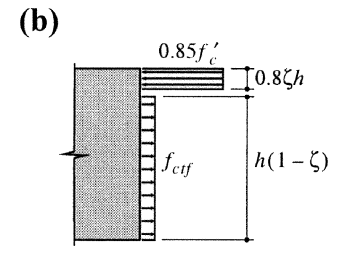


Fig. 7—Uniaxial tension: (a) pullout of randomly oriented fibers; and (b) average stress versus crack opening.





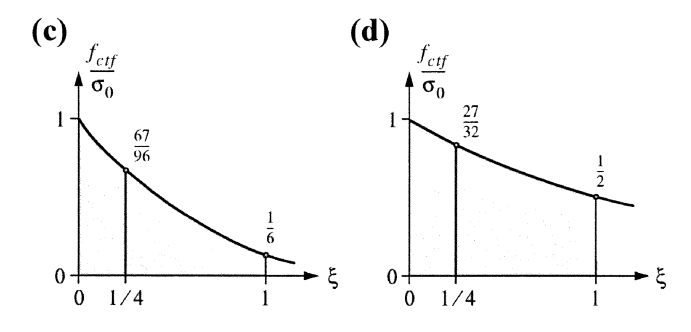


Fig. 8—Flexure: (a) rotation and stress distribution at flexural hinge; (b) nominal stress distribution at flexural hinge; (c) softening assuming z = 0; and (d) effective flexural tensile strength determined from average dissipation.

and using the tensile stress distribution according to Fig. 7(b), we get, for  $0 \le \xi \le 1$ 

$$z = \frac{h}{1 + \frac{2.04 f_c'}{\sigma_0 (3 - 3\xi + \xi^2)}}$$
(7)

and the moment per unit width

$$m = 0.68 f_c' z \left[ 0.6z + (h - z) \frac{6 - 8\xi + 3\xi^2}{12 - 12\xi + 4\xi^2} \right]$$
 (8)

Similarly, for  $\xi > 1$ 

$$z = \frac{h}{1 + \frac{2.04 f_c' \xi}{\sigma_0}}$$
 (9)

and

$$m = 0.68 f_c' z \left( 0.6z + \frac{h - z}{4\xi} \right)$$
 (10)

Note that  $\xi = 1$  implies that all fibers have been pulled out at the open end of the crack.

Assuming a nominal stress distribution<sup>20</sup> as shown in Fig. 8(b), with a uniform, effective flexural tensile strength  $f_{ctf}$  over the depth  $h(1 - \zeta)$  and a compressive stress of  $0.85f_c'$  over 80% of the depth  $\zeta h$  one obtains

$$f_{ctf} = f_c' \frac{0.68\zeta}{1 - \zeta} \tag{11}$$

with

$$\zeta = \sqrt{6.25 + \frac{m}{0.068h^2 f_c'}} - 2.5 \tag{12}$$

Thus, for any assumed  $\xi$ , the compression zone depth z and the associated moment m can be found from Eq. (7) or (9) and (8) or (10), respectively, and, by using Eq. (6), (11), and (12), the corresponding effective flexural tensile strength  $f_{ctf}$  can be determined.

# Flexure—Approximate analysis

Neglecting the small depth z of the compression zone Eq. (7) and (8) result in

$$m = \frac{\sigma_0 h^2 (6 - 8\xi + 3\xi^2)}{12} \tag{13}$$

for  $0 \le \xi = 2\theta h/l_f \le 1$ . Similarly, for  $\xi > 1$ , Eq. (9) and (10) yield

$$m = \frac{\sigma_0 h^2}{12\xi^2} \tag{14}$$

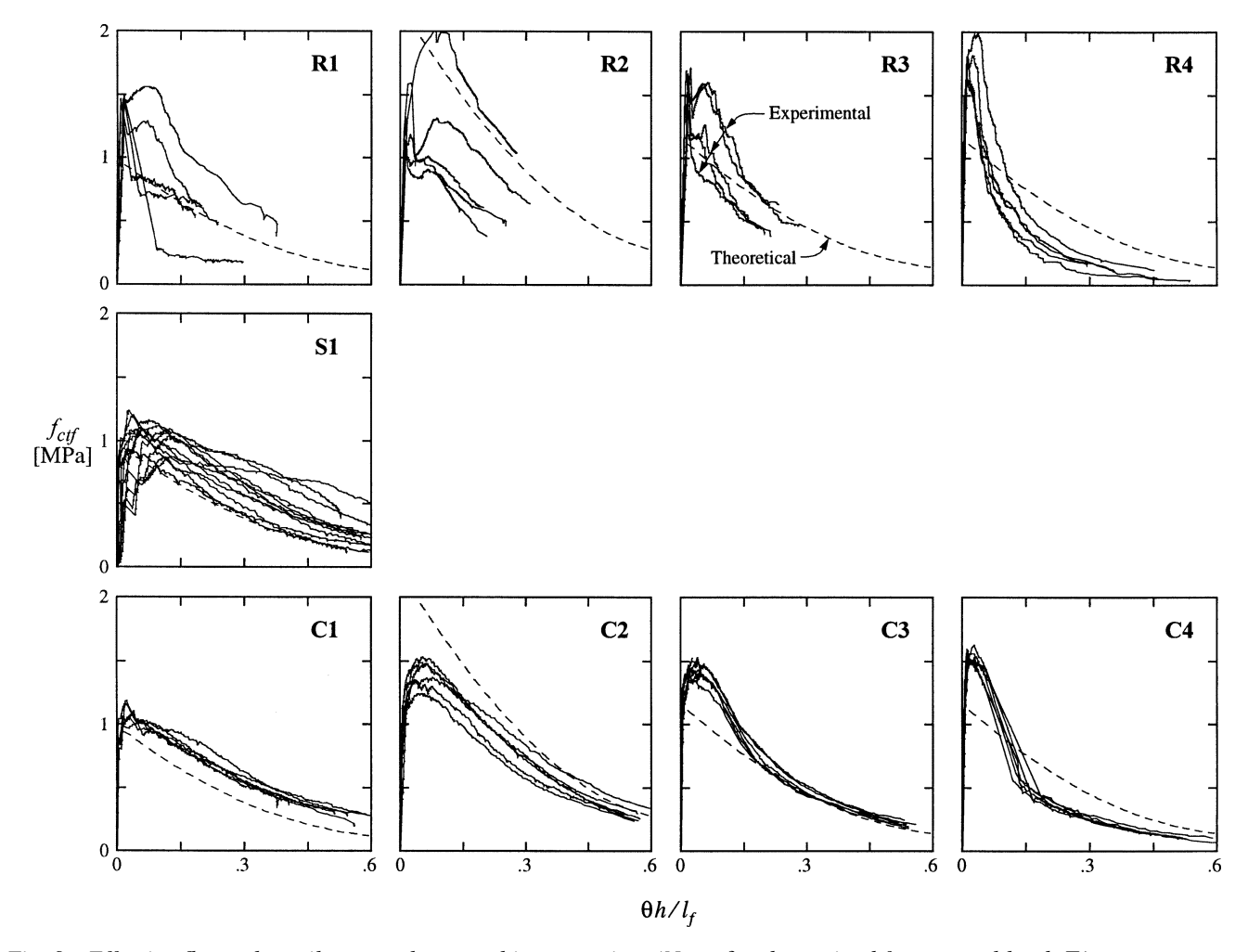
Noting that

$$f_{ctf} = \frac{2m}{h^2} \tag{15}$$

the diagram shown in Fig. 8(c) is obtained.

Accounting for Eq. (4), the dissipation per unit length of the flexural hinge equals

$$\int_{0}^{\theta} md\theta = \int_{0}^{\xi} \frac{ml_{f}}{2h} d\xi = \frac{G_{f}h(6\xi - 4\xi^{2} + \xi^{3})}{4}$$
 (16)



 $\textit{Fig. 9--Effective flexural tensile strength versus hinge rotation.} \ (\textit{Note:} \ f_{ctf} \ \textit{determined from actual loads} \ F.)$ 

for  $0 \le \xi \le 1$  and

$$\int_{0}^{\theta} md\theta = \int_{0}^{\xi} \frac{ml_f}{2h} d\xi = G_f h \left( 1 - \frac{1}{4\xi} \right)$$
 (17)

for  $\xi > 1$ 

Instead of determining  $f_{ctf}$  from actual values of m, average values of m according to Eq. (16) and (17) may be used, hence

$$f_{ctf} = \frac{\sigma_0(6 - 4\xi + \xi^2)}{6} \tag{18}$$

for  $0 \le \xi \le 1$  and

$$f_{ctf} = \frac{\sigma_0(4\xi - 1)}{6\xi^2} \tag{19}$$

for  $\xi > 1$ , refer to Fig. 8(d).

# Comparison with experiments

Considering a rigid-softening plastic behavior according to the failure mechanisms illustrated in Fig. 1, the different tests can be analyzed in a unified manner.

For the modulus of rupture test (Fig. 1(a)), the displacement  $w = w_m l/(3x)$  corresponds to the hinge rotation

$$\theta = \frac{6w}{l} \tag{20}$$

and the associated moment per unit width is found from

$$m = \frac{Fl}{6h} \tag{21}$$

Thus, using Eq. (11) and (12),  $f_{ctf}$ - $\theta$  curves can be plotted as shown in Fig. 9 (Series R1 through R4). The dashed lines correspond to theoretical predictions according to the general analysis outlined previously.

For the square slab test with eight cracks, as shown in Fig. 1(b), the hinge rotation between adjoining slab segments equals

$$\theta = \frac{2w\sqrt{2-\sqrt{2}}}{b-a\sqrt{2}} \tag{22}$$

and the associated moment per unit slab width is determined by

$$m = \frac{F(b - a\sqrt{2})}{16(\sqrt{2} - 1)(b + 2c)}$$
 (23)

For the case of four diagonal cracks extending from the slab center to the slab corners

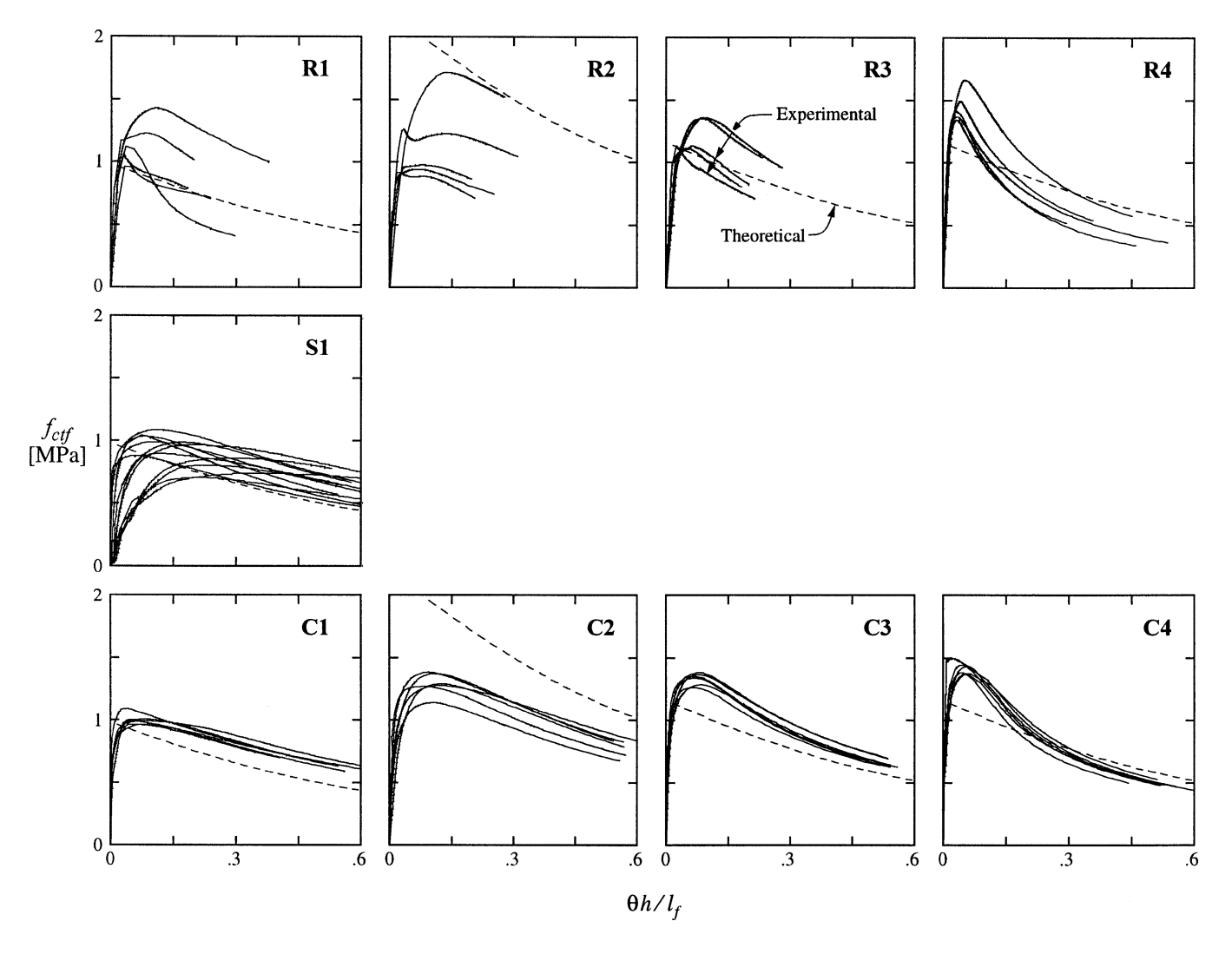


Fig. 10—Effective flexural tensile strength versus hinge rotation. (Note: f<sub>ctf</sub> determined from average loads W/w.)

$$\theta = \frac{2w\sqrt{2}}{b-a}$$

$$m = \frac{F\left[b\cos\left(\frac{\pi}{n}\right) - a\right]}{2n(b+2c)\sin\left(\frac{\pi}{n}\right)}$$
(27)

and

$$m = \frac{F(b-a)}{8(b+2c)}$$
 (25)

For cases with five to seven cracks one may either adopt a linear approximation<sup>20</sup> between the values given by Eq. (22) and (24), and (23) and (25), respectively, or a separate analysis for the actually observed crack pattern may be performed. Figure 9 compares test results (Series S1) with corresponding theoretical predictions.

For the circular slab test shown in Fig. 1(c)

$$\theta = \frac{4w \sin\left(\frac{\pi}{n}\right)}{b \cos\left(\frac{\pi}{n}\right) - a} \tag{26}$$

and

where n = number of cracks. Figure 9 presents  $f_{ctf}$   $^{-}\theta$  curves for the four test series (C1 through C4), accounting for the actually observed number of cracks. Again, theoretical predictions according to the general analysis outlined above are included for comparison purposes.

Note that for the analysis of the square and circular slab tests the stiff steel loading plates have been assumed to be rigid and ordinary yield-line analysis<sup>21</sup> has been applied.

The theoretical predictions in Fig. 9 are based on  $l_f = 60d_f$  = 30 mm as well as the concrete strengths and fiber contents reported in Table 2, assuming a steel density of 7850 kg m<sup>-3</sup>. For Mixture 4 the fiber loss through shotcreting amounted to about 20%. Therefore, an effective reinforcement ratio of  $\rho_f$  = 40/7850 = 0.51% has been used in the calculations; any increase of the effective reinforcement ratio due to fiber alignment parallel to the surface has been ignored.

Figure 10 is similar to Fig. 9 but instead of using the actual values of F for the determination of  $f_{ctf}$  associated with w and

 $\theta$ , average values of  $f_{ctf}$  are determined from the average loads W/w for the deflection intervals between 0 and w.

#### Discussion

Similar to Fig. 4, Fig. 9 and 10 exhibit considerable scatter for the modulus of rupture tests. In comparison, the circular slab tests in particular show only little scatter.

For Mixtures 1 and 3, the theoretical curves in Fig. 9 and 10 compare well with the experimental findings. For Mixture 2 with its high fiber content of 90 kg/m<sup>3</sup> of concrete, the theory is unconservative; nonuniform fiber distribution may be the reason for the lower efficiency. The shotcrete specimens made from Mixture 4 exhibit a drastic softening; it was observed<sup>6</sup> that partly, fibers failed rather than having been pulled out.

While the theoretical predictions included in Fig. 9 and 10 are based on the general analysis outlined above it, should be noted that the approximate analysis would have resulted in practically identical predictions.

The unconservative prediction for Mixture 2 demonstrates that  $\sigma_0$  should not be determined from a pure theoretical consideration, that is, by applying Eq. (2) and (5). Instead, it is recommended to determine  $\sigma_0$  (or  $f_{ctf}$ ) experimentally, as described in the following.

Starting from an experimentally determined value  $\sigma_0$ , the softening relationships (3), (13) and (14) or (18) and (19) capture the real behavior with reasonable accuracy.

# SUGGESTED TEST PROCEDURES

# Existing requirements for modulus of rupture tests

Standards<sup>1-3</sup> differ in their requirements regarding specimen geometry and loading procedures. They require evaluation of Eq. (1) for various deflections, and there are considerable differences among the maximum required deflections.

The ASTM Standard C  $1018^1$  requires the determination of the peak load  $F_0$  as well as the associated deflection  $w_0$ . Equation (1) has to be evaluated for  $w_5 = 3w_0$ ,  $w_{10} = 5.5w_0$ , and  $w_{20} = 10.5w_0$ . Then, the associated integrals  $W_5$ ,  $W_{10}$ , and  $W_{20}$ , according to Eq. (1), are compared with  $W_0$  associated with  $w = w_0$ . The  $100 \times 100 \times 350$  mm specimens are subjected to third-point bending with a span of 300 mm. The rate of loading has to be between 0.05 and 0.1 mm/min.

The DBV Recommendation<sup>2</sup> also requires the determination of  $F_0$  and  $w_0$ . Then, the differences of the expressions W according to Eq. (1) for deflections of  $w_0 + 13l/12,000$  and  $w_0 + l/4000$  as well as  $w_0 + 21l/4000$  and  $w_0 + l/4000$  are computed, respectively, to find average loads for these deflection intervals. From the average loads, a nominal tensile stress-strain diagram is established. The 150 x 150 x 700 mm specimens are subjected to third-point bending with a span of 600 mm. The prescribed rate of loading is equal to 0.2 mm/min.

The Japanese Standard SF- $4^3$  requires the evaluation of Eq. (1) for a deflection of w = 1/150 and the determination of the associated average load F = W/w.

# Existing requirements for square slab tests

The EFNARC Specifications<sup>4</sup> require  $600 \times 600 \times 100$  mm square slab specimens to be simply supported along the edges with clear spans of 500 mm in each direction. A single load shall be applied at the slab center via a  $100 \times 100$  mm steel plate. The central deflection shall be increased at a rate of 1.5 mm/min. Eq. (1) shall be evaluated for w = 25 mm, and

the resultant work shall be compared with the value obtained from reference tests on equivalent mesh reinforced specimens.

For a 100 mm thick plate containing a mesh reinforcement in the middle plane with a yield strength of 500 MPa and a cross-sectional area of  $100 \text{ mm}^2$  per m slab width the ultimate moment per unit slab width is approximately equal to 2.45 kN. Thus, using Eq. (23) and the geometrical values introduced previously, the ultimate load can be expected to be equal to 27.2 kN. Hence, assuming a rigid-perfectly plastic behavior, one gets, for w = 25 mm, a dissipation of W = 27.2 x 25 = 680 J, that is, a value of the order of those obtained in our experiments.

# **Proposed test procedures**

Based on our review of existing requirements, testing experience, and theoretical arguments the following requirements are proposed:

- 1. The specimen thickness h should be equal to approximately three times the fiber length  $l_f$  (for example, h = 100 mm for  $20 \text{ mm} \le l_f \le 45 \text{ mm}$ );
- 2. Modulus of rupture test specimens should satisfy the geometrical requirements b = h, c = 3h/4, and l = 9h/2; similarly, a = h, b = 5h, and c = h/2 for the square slab test specimens; and a = h, b = 7h, and c = h/2 for the circular slab test specimens;
- 3. Shotcrete specimens should be prepared in vertical forms; the excess concrete on the rough side in the center of the specimen should be removed by saw-cutting or grinding to obtain a specimen of uniform thickness. Modulus of rupture test specimens should be saw-cut from square slab specimens. It is recommended using the smooth (formwork) side as the supported side during testing for both cast-in-place and shotcrete specimens;
- 4. Specimens shall be loaded in a deformation controlled manner such that the crack opening parameter  $\xi$  according to Eq. (6) increases at a uniform rate of approximately 0.001/s; if peak loads  $F_0$  and associated deflections  $w_0$  are considered to be relevant—either by themselves or for comparison purposes with existing standards—the loading rate up to and somewhat beyond the peak point should be reduced by a factor of 10. The loading and support system shall ensure minimum possible restraints;
- 5. Whereas modulus of rupture tests shall be carried to a deflection  $w_1$  corresponding to a value of  $\xi = 1/4$ , square and circular slab tests shall be terminated at a deflection  $w_2$  corresponding to a value of  $\xi = 1$ ;
- 6. For  $\xi = 1/4$ , the effective flexural tensile strength  $f_{ctf}$  shall be determined from the associated average load,  $W_1/w_1$ ;
  - 7. For  $\xi = 1/4$ , the relationship

$$2F_1 w_1 \ge W_1 \tag{28}$$

shall be satisfied; and

8. For  $\xi = 1$ , the specific fracture energy  $G_f$  derived from the associated work  $W_2$  shall exceed a certain specified value; for example, for structural applications<sup>20</sup>

$$G_f \ge 4 \text{ kNm}^{-1} \tag{29}$$

### **Practical implementation**

Neglecting the small depth z of the compression zone the deflections  $w_1$  corresponding to  $\xi = 1/4 = 2\theta_1 h/l_f$  can be

Table 3—General determination of  $f_{ctf}$  and  $G_f$ 

Test	Modulus	Squar		
type	of rupture	n = 8	n = 4	Circular slab
$w_1$	$\frac{l_f x}{16h}$	$\frac{(b-a\sqrt{2})l_f}{16\sqrt{2}-\sqrt{2}h}$	$\frac{(b-a)l_f}{16\sqrt{2}h}$	$\frac{\left[b\cos\left(\frac{\pi}{n}\right) - a\right]l_f}{32\sin\left(\frac{\pi}{n}\right)h}$
$W_1$	$\frac{l}{3x}\int_{0}^{w_{1}}Fdw$	$\int_{0}^{w_{1}} Fdw$	$\int_{0}^{w_{1}} Fdw$	$\int_{0}^{w_{1}} Fdw$
$f_{ctf}$	$\frac{16W_1}{bhl_f}$	$\frac{2\sqrt{2}+\sqrt{2}W_1}{(b+2c)hl_f}$	$\frac{4\sqrt{2}W_1}{(b+2c)hl_f}$	$\frac{32W_1}{n(b+2c)hl_f}$
$w_2$	$4w_1$	4w <sub>1</sub>	4w <sub>1</sub>	4w <sub>1</sub>
$W_2$	$\frac{1}{3x}\int_{0}^{w_{2}}Fdw$	$\int_{0}^{w_{2}} Fdw$	$\int_{0}^{w_{2}} Fdw$	$\int_{0}^{w_{2}} Fdw$
$G_f$	$\frac{4W_2}{3bh}$	$\frac{\sqrt{2+\sqrt{2}}W_2}{6(b+2c)h}$	$\frac{\sqrt{2}W_2}{3(b+2c)h}$	$\frac{8W_2}{3n(b+2c)h}$

Table 4—Practical determination of  $f_{ctf}$  and  $G_f^*$ 

Test type	Modulus of rupture	Square slab	Circular slab
Recommended no. of tests	≥15	≥3	≥3
а	_	h	h
b	h	5 <i>h</i>	7 <i>h</i>
С	3 <i>h</i> /4	h/2	h/2
l	9h/2	_	_
$w_1$	$\frac{l_f x}{16h}$	$(0.03n + 0.06)l_f$	$(0.07n - 0.10)l_f$
$f_{ctf}$	$\frac{12W_1}{h^2l_f}$	$(0.95 - 0.06n) \frac{W_1}{h^2 l_f}$	$\frac{3W_1}{nh^2l_f}$
$G_f$	$\frac{4W_2}{3h^2}$	$(0.107 - 0.007n) \frac{W_2}{h^2}$	$\frac{W_2}{3nh^2}$

<sup>\*</sup> $f_{ctf}$  values reduced by a factor of 3/4 to account for scatter. <sup>20</sup>

computed from Eq. (6), (20), (22), (24), and (26). From the associated amounts of work  $W_1$ , one obtains

$$f_{ctf} = \frac{16W_1}{A_{cr}l_f} \tag{30}$$

since  $W_1 = A_{cr} f_{ctf} (h/2) \theta_1$ , where  $A_{cr} =$  total crack area. According to Eq. (16) and (17), 75% of the fracture energy have been dissipated for  $\xi = 1$ , hence

$$G_f = \frac{4W_2}{3A_{cr}} \tag{31}$$

In summary, the relationships given in Table 3 are obtained.

Considering the geometrical requirements stated previously, adopting a linear approximation for the influence of n in the square slab tests, and introducing a reduction factor of 3/4 to account for the scatter in the  $f_{ctf}$  values, Table 4 is established.<sup>20</sup>

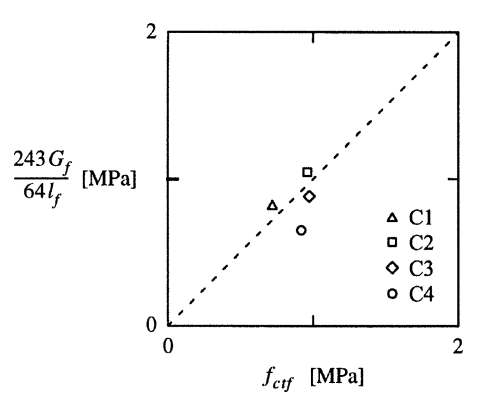


Fig. 11—Comparison of effective flexural tensile strengths determined from circular slab tests.

### **Discussion**

For h = 100 mm, the proposed dimensions of the modulus of rupture test specimens are between those required by ASTM<sup>1</sup> and DBV.<sup>2</sup> The proposed ultimate deflection is approximately equal to that required by the Japanese Standard,<sup>3</sup> but somewhat greater than the values required by ASTM<sup>1</sup> and DBV.<sup>2</sup> Unless peak loads  $F_0$  and associated deflections  $w_0$  are considered to be relevant, the proposed loading rate is approximately five to 10 times faster than required by these standards. Contrary to  $F_0$  and  $w_0$ ,  $W_1$  is not very sensitive to the loading rate.<sup>5,6</sup>

The proposed square slab test procedures are very similar to those required by EFNARC. For h = 100 mm,  $l_f = 30 \text{ mm}$ , and n = 5, Table 4 results in  $w_2 = 25.2 \text{ mm}$ , and the required rate of loading is equivalent to a deflection increase of 60 x 25.2/1000 = 1.51 mm/min.

Equation (28) aims at excluding materials with a too drastic softening. For example, Mixture 4 of the present tests would be excluded by this criterion. Note that, theoretically, according to Fig. 8(c) and (d), the quotient  $F_1w_1/W_1$  is equal to 67/81, that is, 60% greater than the required minimum of 0.5.

Similar to Eq. (29), other requirements could be introduced to classify steel fiber-reinforced concrete.

Whereas Reference 20 does not allow for the determination of  $G_f$  from modulus of rupture tests, corresponding expressions have been included in Tables 3 and 4 for the sake of completeness.

For  $\xi = 1/4$ , Eq. (4) and (18) result in  $G_f = 16 f_{ctf} l_f / 81$  or, if one accounts for the reduction factor<sup>20</sup> of 3/4 included in  $f_{ctf}$ 

$$G_f = \frac{64 f_{ctf} l_f}{243} \tag{32}$$

Thus,  $G_f$  can approximately be determined from  $f_{ctf}$ , or vice versa, if only one of the two values is available. For example, except for Series C4, Eq. (32) provides a reasonable approximation for the circular slab tests (Fig. 11).

### **DESIGN RECOMMENDATIONS**

In general, both ultimate and serviceability limit states should be considered.<sup>20</sup>

Regarding ultimate strength, sectional forces and moments may be determined from an elastic analysis or from any other solution satisfying equilibrium. For permanent loading and situations of high risk, the deformation behavior should be investigated, accounting for the inherent softening response of steel fiber-reinforced concrete. For

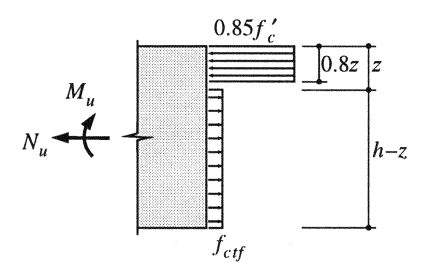


Fig. 12—Nominal stress distribution under ultimate axial force and bending moment.

flexure and axial load, computation of the sectional resistances  $M_u$  and  $N_u$  can be based on the nominal stress distribution shown in Fig. 12 where  $f_{ctf}$  is determined according to Table 4; factored moments and forces should not exceed reduced resistances, accounting for a strength reduction factor<sup>20</sup> of 5/6.

Regarding serviceability, sectional forces and moments should be determined from an elastic analysis. Extreme fiber tensile stresses in pure flexure should be limited to  $2f_{ctf}$ , whereas for pure axial tension, a limitation to  $2f_{ctf}/3$  is recommended.<sup>20</sup> Note that, according to Eq. (18) and because of the reduction factor of 3/4 included in the  $f_{ctf}$  values of Table 4, the stress limitation of  $2f_{ctf}/3$  corresponds to a safety factor of 64/27 against reaching the average value of  $\sigma_0$ ; according to Eq. (15), the (elastic) extreme fiber tensile stress  $6m/h^2$  of  $2f_{ctf}$  in pure flexure corresponds to a uniform tensile stress of  $2f_{ctf}/3$ , similar to pure axial tension.

### **CONCLUSIONS**

The circular slab tests provide a valuable alternative to the modulus of rupture and square slab tests. They exhibit little scatter and are easy to execute and analyze. Therefore, they are particularly suited for routine on-site quality control.

Similar to the Japanese and EFNARC specifications, 3,4 the proposed test procedures emphasize the softening response after cracking. Unlike the American and German requirements, 1,2 they do not rely on the determination of peak loads and associated deflections.

For the design of steel fiber-reinforced concrete members, it is proposed to use the effective flexural tensile strength  $f_{ctf}$ determined from the average load  $W_1/w_1$  at a nominal deformation of  $\xi = 1/4$ , as the basic strength parameter.

The proposed criterion  $2F_1w_1 \ge W_1$  for  $\xi = 1/4$  aims at excluding materials with a too drastic softening. It is rather strict and may be revised based on future findings.

Specifying the work dissipated in a slab test corresponds to requiring a certain specific fracture energy  $G_f$  and allows for the classification of different steel fiber-reinforced concretes.

The present experiments are restricted to a relatively narrow range of parameters and to one fiber type. Future work should be directed at defining the limits of applicability of the approaches advanced in this paper.

#### ACKNOWLEDGMENTS

This paper resulted from a research project accompanying the development of a Swiss recommendation for steel fiber-reinforced concrete. Financial support from the Swiss National Science Foundation and ETH Zurich is gratefully acknowledged.

# NOTATION

area = crack area

dimension of loading plate

span length of slab, beam width

length of overhang fiber diameter

maximum aggregate diameter

applied load peak load

concrete cylinder compressive strength

concrete tensile strength effective flexural tensile strength

specific fracture energy

member depth span length

 $M_u$ fiber length flexural resistance

bending moment per unit width

 $N_u$ axial force resistance number of cracks crack opening и W work done by F

 $W_1, W_2 =$ work corresponding to  $w_1$  and  $w_2$ 

deflection at loading points

deflections corresponding to  $\xi = 1/4$  and  $\xi = 1$  $w_1, w_2 =$ 

deflection associated with  $F_0$  $w_0$ 

 $w_m$ deflection at midspan

distance of flexural hinge from nearer support x

= compression zone depth

θ hinge rotation

 $\theta_1$ hinge rotation corresponding to  $\xi = 1/4$ 

 $\sigma$ volumetric reinforcement ratio

axial stress =  $\sigma_0$ initial stress bond shear stress  $\tau_b$ 

crack opening parameter

compression zone depth parameter

# REFERENCES

1. ASTM C 1018-97, "Standard Test Method for Flexural Toughness and First-Crack Strength of Fiber-Reinforced Concrete (Using Beam with Third-Point Loading)," ASTM, Philadelphia, PA, 1997, 8 pp.

2. DBV, DBV-Merkblätter Faserbeton (DBV Recommendation on Fiber-Reinforced Concrete), Deutscher Beton-Verein E.V., 1992, 43 pp

3. JCI, JCI Standards for Test Methods of Fiber-Reinforced Concrete, JCI-SF, Japan Concrete Institute, 1984, pp. 57-59 and 65-68.

4. EFNARC, "Specification for Sprayed Concrete," Final Draft, European Federation of National Associations of Specialist Contractors and Material Suppliers for the Construction Industry, Hampshire, UK, Oct.

5. Pfyl, T., "Versuche an Stahlfaserbetonplatten und -balken (Tests on Steel Fiber-Reinforced Concrete Slabs and Beams)," Diploma thesis, ETH Zürich, Switzerland, Jan. 1997.

6. Ulaga, T., "Biegeverhalten von Stahlfaserbeton (Flexural Response of Steel Fiber-Reinforced Concrete)," Diploma thesis, ETH Zürich, Switzerland, June 1997.

7. Hartwich, K., Zum Riss- und Verformungsverhalten von stahlfaserverstärkten Stahlbetonstäben unter Längszug (Cracking and Deformation Behavior of Steel Fiber-Reinforced Concrete Tension Members), Institut für Baustoffe, Massivbau und Brandschutz, Technische Universität Braunschweig, 1986, 202 pp.

8. Körmeling, H. A., "Impact Tensile Strength of Steel Fiber Concrete," Report 5-84-8, Stevin Laboratory, TH Delft, July 1984, 149 pp.

9. Shah, S. P.; Stroeven, P.; Dalhuisen, D.; and van Stekelenburg, P., "Complete Stress-Strain Curves for Steel Fiber-Reinforced Concrete in Uniaxial Tension and Compression," Proceedings, Rilem Symposium 1978, Testing and Test Methods of Fiber Cement Composites, R. N. Swamy, ed., Construction Press Ltd., Lancaster, England, 1978, pp. 399-408.

10. Aveston, J., and Kelly, A., "Theory of Multiple Fracture of Fibrous Composites," Journal of Materials Science, V. 8, 1973, pp. 352-362.

11. Naaman, A. E., and Shah, S. P., "Pullout Mechanism in Steel Fiber-Reinforced Concrete," Journal of the Structural Division, ASCE, V. 102, Aug. 1976, pp. 1537-1548.

12. Maage, M., "Interaction between Steel Fibers and Cement Based Matrixes," Materials and Structures, V. 10, No. 59, 1977, pp. 297-301.

13. Banthia, N., and Trottier, J.-F., "Concrete Reinforced with Deformed Steel Fibers—Part 1: Bond-Slip Mechanisms," ACI Materials Journal, V. 91, No. 5, Sept.-Oct. 1994, pp. 435-446.

14. Pinchin, D. J., and Tabor, D., "Interfacial Phenomena in Steel Fiber-Reinforced Cement," Cement and Concrete Research, V. 8, 1978, pp. 15-24 and 139-150.

- 15. Rehm, G., and Zimbelmann, R., "Untersuchung der für die Haftung zwischen Zuschlag und Zementmatrix massgebenden Faktoren (Investigation of the Factors Influencing the Bond between Aggregates and Cement Matrix)," *Deutscher Ausschuss für Stahlbeton*, Heft 283, Wilhelm Ernst & Sohn, Berlin, 1977, 33 pp.
- 16. Gray, R. J., "Analysis of the Effect of Embedded Fiber Length on Fiber Debonding and Pullout from an Elastic Matrix," *Journal of Materials Science*, V. 19, 1984, pp. 861-870 and 1680-1691.
- 17. Sigrist, V., and Marti, P., "Ductility of Structural Concrete: A Contribution," *Proceedings*, Workshop Development of EN 1992 in Relation to New Research Results and to the CEB-FIP Model Code 1990, Czech Technical University, Prague, Oct. 1994, pp. 211-223.
- 18. Kaufmann, W., and Marti, P., "Structural Concrete: Cracked Membrane Model," *Journal of Structural Engineering*, ASCE, V. 124, No. 12, Dec. 1998, pp. 1467-1475.
- 19. Marti, P.; Alvarez, M.; Kaufmann, W.; and Sigrist, V., "Tension Chord Model for Structural Concrete," *Structural Engineering International*, IABSE, V. 8, No. 4, 1998, pp. 287-298.
- 20. SIA, "Empfehlung SIA 162/6, Stahlfaserbeton (Recommendation on Steel Fiber-Reinforced Concrete)," *Schweizerischer Ingenieur- und Architekten-Verein*, 1999, 20 pp.
- 21. Park, R., and Gamble, W. L., *Reinforced Concrete Slabs*, Wiley-Interscience, 1980, 618 pp.